International Journal of Thermophysics, Vol. 4, No. 4, 1983

Hot Strip Determination of the Thermal Conductivity Tensor and Heat Capacity of Crystals

U. Brydsten[1] and G. Bäckström[1]

Received December 12, 1983

A method of determining the principal thermal conductivities and the specific heat capacity for an anisotropic crystal is presented, tested, and discussed. Two parallel metal strips are deposited onto a plane face of the specimen. One strip serves as a heater, the other as a temperature sensor. A pulse of constant dc power is applied to the heater, and the response at the sensor is measured by means of an ac bridge, monitored by a lock-in amplifier. The experiment is on-line with a PDP-11/34 computer system. The expression for the temperature rise in case of infinitely long strips is fitted to the sensor temperature data. In the isotropic case one experiment yields both thermal conductivity and heat capacity. In an anisotropic case experiments have to be performed with two or three different strip orientations, if all principal thermal conductivities are to be determined. A precision of 0.1% is readily obtained, and the method is thus valuable in cases where small changes in thermal conductivity are to be determined. We estimate that the accuracy generally obtainable is about 2% as regards thermal conductivity and heat capacity. The accuracy in determining thermal diffusivities is mainly limited by geometrical factors and may ultimately be better than 1%. Results are given for isotropic CaF_2 and anisotropic SiO_2 at 300 K.

KEY WORDS: calcium difluoride (CaF_2); heat capacity; silicon dioxide (α–SiO_2); thermal conductivity tensor; thermal diffusivity.

1. INTRODUCTION

It has been shown that thermal conductivity tensor components may be determined, as well as specific heat capacity, by means of a transient method [1]. The specimen is split or ground, so that a plane surface is obtained, containing two principal axes of the thermal conductivity ellipsoid. On this surface two metal strips are deposited parallel to one of the axes. The strips are provided with potential taps as shown in Fig. 1. The longer strip is used as a heater, the shorter one as a resistive temperature

[1] Department of Physics, University of Umeå, S-901 87 Umeå, Sweden.

0195-928X/83/1200-0369$03.00/0

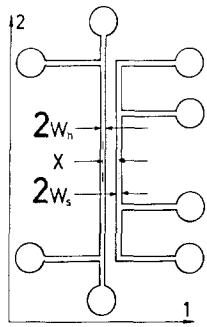

Fig. 1. Pattern of copper and nickel strips deposited on crystal specimen by means of electron beam evaporation. Directions 1 and 2 are principal axes of the thermal conductivity tensor.

sensor. A constant power is applied to the heater, and the response is measured by means of a sensor as a function of time. The thermal quantities may then be calculated from the temperature data. The method was recently used by the present authors [2,3] in investigations of the influence of uniaxial stress on lattice thermal conductivity. Another group has demonstrated the use of a single strip [4], analogous to the hot-wire method, for measuring thermal properties in the anisotropic case. The purpose of this paper is to describe how two-strip experiments may be implemented and to discuss sources of error. The potential for absolute measurements will be illustrated by results on isotropic as well as anisotropic specimens.

2. THEORY OF MEASUREMENTS

2.1. Infinite Heater

Let the principal tensor axis perpendicular to the strips be number *1*, that parallel to the strips number *2*, and that perpenducular to the face number *3*. The expression for the temperature rise at a distance ξ from the center of the heater strip is [1]

$$\Delta T = T - T_0 = q(\lambda_1\lambda_3)^{-1/2} f(\lambda_1 t/\rho c_p, \xi, w_h) \tag{1}$$

where

$$f(\lambda_1 t/\rho c_p, \xi, w_h)$$

$$= (\lambda_1 t/\pi\rho c_p)^{1/2}(2w_h)^{-1}$$

$$\times \left\{\operatorname{erf}(z_+) - \operatorname{erf}(z_-) - z_+ Ei(-z_+^2)\pi^{-1/2} + z_- Ei(-z_-^2)\pi^{-1/2}\right\}$$

Here

$$z_+ = (\rho c_p/4\lambda_1 t)^{1/2}(\xi + w_h), \qquad z_- = (\rho c_p/4\lambda_1 t)^{1/2}(\xi - w_h)$$

q is the power per unit length, λ_i is the thermal conductivity in direction i, t is the time, ρc_p is the heat capacity per unit volume, and w_h is the heater half-width. The expression was derived on the assumptions that the heater strip has no heat capacity and is infinitely long. It was also assumed that the power density is constant over the heater area.

The sensor conductance, G, is assumed to vary linearly with T over the increment produced by the pulse:

$$G = G_0\{1 - \beta(T_0)\Delta T\}$$

where the constant G_0 and the function $\beta(T_0)$ may be determined before the transient experiment. If the sensor has a half-width of w_s, we have the following expression for the sensor conductance in response to a step power:

$$G = (2w_s)^{-1}\int_{x-w_s}^{x+w_s} G_0(1 - \beta(T_0)\Delta T)\,d\xi$$

Using Eq. (1) we finally obtain

$$\begin{aligned}\frac{G_0 - G}{G_0} &= \frac{\beta(T_0)}{2w_s}\int_{x-w_s}^{x+w_s}\Delta T\,d\xi \\ &= \frac{\beta(T_0)q(\lambda_1\lambda_3)^{-1/2}}{2w_s}\int_{x-w_s}^{x+w_s} f(\lambda_1 t/\rho c_p, \xi, w_h)\,d\xi \end{aligned} \tag{2}$$

$$(G_0 - G)/G_0 = \beta(T_0)q(\lambda_1\lambda_3)^{-1/2}F(\lambda_1 t/\rho c_p, x, w_h, w_s)$$

The quantity $(G_0 - G)/G_0 \equiv \Delta R/(R_0 + \Delta R)$, where R is the sensor resistance, may be measured against time by means of a bridge. The two parameters $A_1 = (\lambda_1\lambda_3)^{1/2}$ and $A_2 = \lambda_1/\rho c_p$ may then be determined by fitting the theoretical expression (2) to the measured data. If *1* and *3* are thermally equivalent directions, we immediately have $\lambda_1 = \lambda_3 = A_1$ and $\rho c_p = A_1/A_2$.

If a similar experiment is carried out with the strips parallel to the *1* direction, the fitting procedure yields the parameters $B_1 = (\lambda_2\lambda_3)^{1/2}$ and $B_2 = \lambda_2/\rho c_p$. From this we now obtain $\lambda_2 = B_1^2/A_1$ and $\lambda_2 = B_2A_1/A_2$ (alternatively $\lambda_3 = B_1^2A_2/B_2A_1$). If the three principal tensor components are all different, an additional measurement must be carried out on a crystal face perpendicular to the first one.

Various simplifications are possible in special situations. If ρc_p is already accurately known from other measurements, two independent

values of λ are obtained from a strip measurement on an isotropic material. One of the values depends on β, determined prior to the pulse experiment, but the parameter A_2 yields a conductivity value independent of β and depending only on the uncalibrated bridge output, on time and on geometry. The latter method of determining λ by way of the thermal diffusivity seems to hold promise of high accuracy. If the tensor ellipsoid has axial symmetry and ρc_p is known, a measurement with one strip orientation suffices to determine λ_1 and λ_3. The coefficient β must, however, be determined separately.

In order to reduce calculation times, we store a table of the function $F(\lambda_1 t/\rho c_p, x, w_h, w_s)$, numerically integrated for fixed values of x, w_h, and w_s, in the computer. Values of F for any argument $\lambda_1 t/\rho c_p$ is then quickly obtained by parabolic interpolation. The fitting of Eq. (2) is made by Gauss' method [5] involving successive linerization of the fitting function.

2.2. Finite Heater Length

The above theory is strictly valid only for an infinitely long heater. Since the conduction problem is linear, we should thus subtract, in Eq. (2), the temperature rise that would be produced by the missing heater ends. In practice this contribution can usually be made negligible by a suitable choice of the geometrical parameters, but we need an expression for the end effect in order to check whether the heater is sufficiently long for a given pulse duration. Obviously, it is sufficient to approximate the ends of the heater strip by line sources and to calculate the average temperature along the center line of the sensor, at distance x. According to Carslaw and Jaeger [6] the temperature rise at $x, y, 0, t$ due to an instantaneous point source at $x', y', 0, t'$ of energy E is (with $c \equiv c_p$)

$$\Delta T_E = \frac{E(\rho c)^{1/2}}{4\pi^{3/2}(t-t')^{3/2}(\lambda_1\lambda_2\lambda_3)^{1/2}} \times \exp\left\{-\frac{\rho c}{4(t-t')}\left[\frac{(x-x')^2}{\lambda_1} + \frac{(y-y')^2}{\lambda_2}\right]\right\}$$

Integrating this expression over t' we obtain the response to a continuous point source of power P at $x' = 0$:

$$\Delta T_p = \frac{p}{2\pi(\lambda_1\lambda_2\lambda_3)^{1/2}}\left[\frac{x^2}{\lambda_1} + \frac{(y-y')^2}{\lambda_2}\right]^{-1/2} \operatorname{erfc}\left\{\frac{\rho c}{4t}\left[\frac{x^2}{\lambda_1} + \frac{(y-y')^2}{\lambda_2}\right]\right\}^{1/2} \tag{3}$$

If the heater extends to $\pm L_h$ and the potential taps of the sensor are at $\pm L_s$, we have the following expression for a finite heater:

$$\frac{G_0 - G}{G_0} = \frac{\beta(T_0)}{2w_s} \int_{x-w_s}^{x+w_s} \Delta T \, d\xi - \frac{\beta(T_0)}{2L_s} \int_{-L_s}^{+L_s} dy \int_{L_h}^{\infty} 2\Delta T_p \, dy' \qquad (4)$$

with $q\,dy'$ replacing P in ΔT_p. The double integral must be evaluated numerically, but only modest accuracy is required to estimate the ratio of the error term to the total.

So far we have considered the effect of the absence of heater strip for $|y'| > L_h$. In the practical case there are, however, also soldering points at the ends, which tend to maintain the temperature at its initial value. For the worst case of zero temperature increase at the soldering points, acceptable boundary conditions are obtained with the following model. A finite strip source of strength q is combined with strip sources of strength $-q$, extending from the limits to infinity. If we let $y' = 0$ be a soldering point, the temperature perturbation ΔT_e for $y > 0$ is given by an integral over the continuous point source solution (Eq. 3):

$$\Delta T_e = \int_{-W_h}^{W_h} dx' \int_{-\infty}^{0} dy' \, \Delta T_p \qquad (5)$$

which has to be computed numerically.

A rough estimate of the cooling caused by a solder point may be obtained in a much simpler way. According to Eq. (1) the heater temperature at $\xi = 0$ varies slowly for large times. If the heater temperature is approximated by the maximum value, $\Delta T_{\max}$, the perturbation is given by the well-known solution [6]

$$\Delta T_e = \Delta T_{\max} \operatorname{erfc}\left[y/2(\lambda_2/\rho c t)^{1/2} \right] \qquad (6)$$

2.3. Finite Mass of Strips

The thermal lag caused by the finite heat capacity of the heater strip may be estimated using the line source as an approximation. The power stored in the strip is $m_h c_h \dot{T}$, m_h being the mass per unit length and c_h the specific heat per unit mass of the heater material. This power will not be available for conduction in the specimen and effectively yields a negative contribution to q in Eq. (1). Using superposition we treat the response to this contribution as a temperature deficit. The average temperature of the heater may be approximated by that in the middle, ΔT_m, and hence we have $\dot{T}(t') = d(\Delta T_m)/\partial t'$, with

$$\Delta T_m = q(\lambda_1 \lambda_3)^{-1/2} f(\lambda_1 t'/\rho c, 0, w_h).$$

Integrating over instantaneous line sources [6], dissipating the power deficit $m_h c_h \dot{T}$, we obtain an expression for the temperature deficit, δT_h, which may be transformed by partial integration

$$\delta T_h = \frac{m_h c_h}{2\pi(\lambda_1\lambda_3)^{1/2}} \int_0^t \frac{d\Delta T_m}{dt'} \frac{1}{t-t'} \exp\left[-x^2\rho c/4\lambda_1(t-t')\right] dt'$$

$$= \frac{m_h c_h}{2\pi(\lambda_1\lambda_3)^{1/2}} \int_0^t \Delta T_m \left[\frac{x^2\rho c}{4\lambda_1(t-t')^3} - \frac{1}{(t-t')^2} \right]$$

$$\times \exp\left[-x^2\rho c/4\lambda_1(t-t')\right] dt' \tag{7}$$

This final expression may be integrated numerically. In practice the power deficit is large only at small times and can hence also be treated very roughly in terms of a time shift, δt, obtainable from $q\,\delta t = m_h c_h \Delta T_{\max}$, where ΔT_{max} is the temperature at the end of the pulse.

The effect of finite sensor mass may be estimated in a similar fashion. The temperature at the middle of the sensor, ΔT_s, is approximately given by the continuous line source solution [1],

$$\Delta T_s = \frac{q}{2\pi(\lambda_1\lambda_3)^{1/2}} \int_{x^2\rho c/4\lambda_1 t}^{\infty} \frac{e^{-u}}{u}\, du \tag{8}$$

and the sensor heating rate thus becomes

$$\dot{T}_s(t') = \frac{q}{2\pi(\lambda_1\lambda_3)^{1/2} t'} \exp\left(-x^2\rho c/4\lambda_1 t'\right) \tag{9}$$

The solution corresponding to the instantaneous strip source is obtained by integrating over instantaneous line sources as follows:

$$\Delta T_{is} = \frac{E/2w_s}{2\pi t(\lambda_1\lambda_3)^{1/2}} \int_{-w_s}^{w_s} \exp\left[-(\xi-\xi')^2\rho c/4\lambda_1 t\right] d\xi'$$

$$= \frac{E}{4\pi^{1/2} t^{1/2} \lambda_3^{1/2} (\rho c)^{1/2} w_s} \left[\operatorname{erf}(z_+) - \operatorname{erf}(z_-)\right]$$

with the notation $z_\pm = (\rho c/4\lambda_1 t)^{1/2}(\xi \pm w_s)$. In this expression we put $\xi = 0$, since we are interested in the temperature at the center of the sensor. We now estimate the temperature deficit, δT_s, at the sensor by integrating ΔT_{is}

over t' using the energy deficit $E = m_s c_s \dot{T}_s \, dt'$:

$$\delta T_s = A \int_0^t \frac{1}{t'} \exp(-x^2 \rho c / 4\lambda_1 t') \left(\frac{1}{t - t'} \right)^{1/2} \operatorname{erf} \left[\frac{\rho c w_s^2}{4\lambda_1 (t - t')} \right]^{1/2} dt'$$

$$A = \frac{q m_s c_s}{4\pi^{3/2} \lambda_1^{1/2} \lambda_3 (\rho c)^{1/2} w_s} \tag{10}$$

An upper limit to the above integral expression for δT_s may be obtained. We note that $\dot{T}_s(t')$ in Eq. (9) has a maximum value of $4q\lambda_1 / (2\pi e x^2 \rho c \lambda_1^{1/2} \lambda_3^{1/2})$ and that the last factor in Eq. (10) is positive. Taking $\dot{T}_s(t')$ equal to its maximum value, we thus obtain an upper limit to the integral in Eq. (10), which then corresponds to a continuous strip source. Putting $q = m_s c_s \dot{T}_{\max}$ and $\xi = 0$ in Eq. (1), we finally have

$$\delta T_s < 2 m_s c_s q / (\pi e x^2 \rho c \lambda_3) f(\lambda_1 t / \rho c, 0, w_s) \tag{11}$$

3. EXPERIMENTAL PROCEDURE

The timing circuitry consists of an oscillator, a frequency divider, and a triple counter (Fig. 2). The oscillator and the current amplifier AO supply ac to the bridge, designed to detect the change in sensor resistance. The

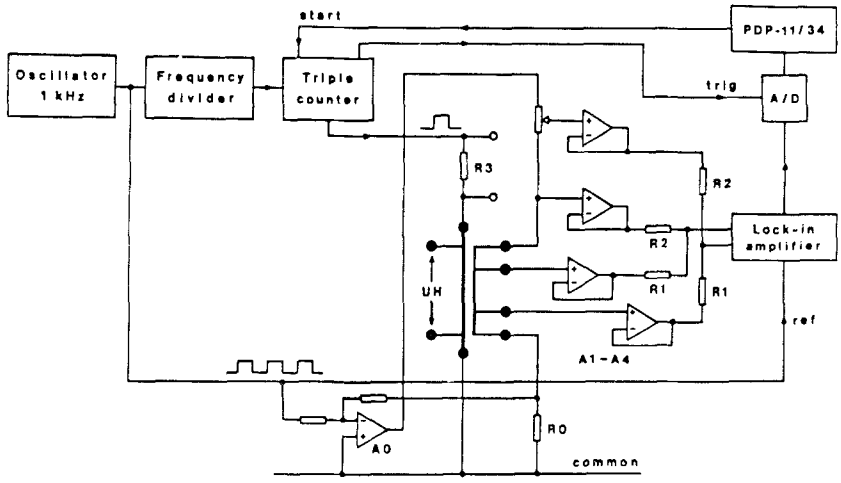

Fig. 2. Circuitry for heating and temperature sensing.

frequency divider sets the time interval between samples of the lock-in amplifier output. The triple counter delivers selected numbers of trigger pulses to the A/D converter. (Conversion was performed by a Hewlett–Packard 3456A multimeter at the later stages of this work.) First, a certain number of background points are taken without heating. Then dc is supplied to the heater, and readings are taken until the end of the heating pulse. Finally, a number of points are taken during cooling, still at the same rate.

The triple counter also delivers a voltage pulse of constant height for the heater strip. The series resistor, R3, is chosen equal to the total resistance of the heater strip, so the power developed in the heater remains constant to first order. The resistance of the sensor strip is typically of the order of 300 Ω. The low noise amplifiers A1–A4 of unity gain transform impedances, so that reasonably low bridge resistance values may be used. The bridge is essentially of Kelvin–Thomson type.

Measurements are started on command from the PDP-11/34 computer, which is also used to manage the A/D converter and to calculate values of λ and ρc_p. When the measured sensor resistance values have been stored in memory, the next step is to fit a straight line to the background points (Fig. 3). Values calculated by extrapolating this line are subtracted from those obtained on heating, yielding the net resistance rise (Fig. 4). Equation (2) is then fitted to these reduced resistance values in order to

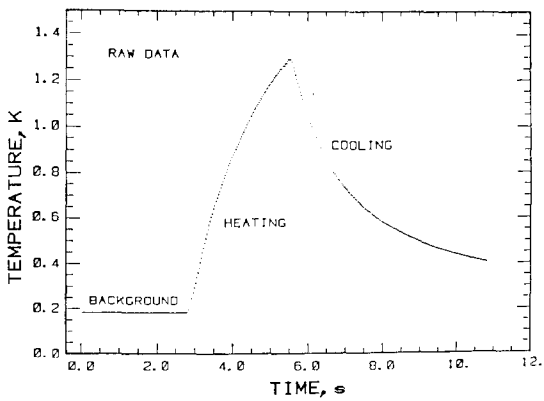

Fig. 3. Raw data obtained at the output of the lock-in voltmeter. The first part of the curve (90 points) corresponds to the sensor temperature before heating (background), the second part (90 points) to the temperature rise on heating. These two phases are used for analysis in this paper. The cooling phase could also be used, if the strips had been long enough to avoid end effects.

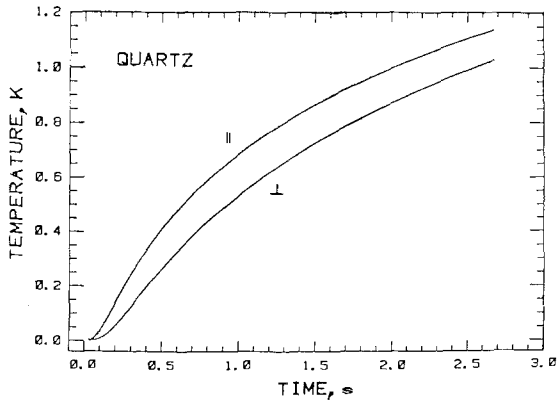

Fig. 4. Reduced temperature data and best fitting theoretical curves corresponding to the two principal strip orientations on quartz. The 180 data points fall mostly on the curves.

find the thermal parameters. We have not so far utilized the temperature data measured on cooling, although a corresponding fitting function may readily be obtained from Eq. (2) by subtracting a delayed solution of the same kind.

Equation (2) is obviously nonlinear in the parameters $A_1 = (\lambda_1\lambda_3)^{1/2}$ and $A_2 = \lambda_1/\rho c_p$, from which λ_i and ρc_p are to be calculated. Fitting is achieved by Gauss' classical method [5], involving first order Taylor expansion of the fitting function in each iteration. This method was slightly modified by limiting the step length in parameter space. In order to avoid repeated calculations of the function F in Eq. (2) during fitting, we tabulate it for given x, w_h, and w_s and use parabolic interpolation in the single variable $\lambda_1 t/\rho c_p$.

The strips were formed by electron beam evaporation. Copper was used for the heater and nickel for the sensor. The sensor was calibrated by measuring the resistance between its potential taps quasistatically against temperature, determined by a Hewlett–Packard quartz thermometer. At each temperature the resistance was measured repeatedly by a Hewlett–Packard 3456A multimeter, until readings indicated that equilibrium had been reached, which typically required about an hour. The calibration factor that should multiply a measured voltage increment to yield the sensor resistance increment, ΔR, is determined separately. We automatically switch a set of large, parallel resistances over the upper bridge resistor (Fig. 2, resistor with center-tap), thus providing known values of ΔR. This procedure also checks the linearity of the output signal versus ΔR.

4. SOURCES OF ERROR

4.1. Error Related to Geometry

The finite length of the heater contributes an error to the temperatures measured at large times. A safe pulse length may be calculated from the formulas in Sec. 2.2. The temperature error grows strongly at large times, causing a characteristic deviation from Eq. (2), which also provides warning against excessive pulse time. The ratio of heater length to strip separation could be increased to permit the use of longer times. The potential taps on the heater locally reduce the power dissipated at the junction. The temperature perturbation caused by this deficit will, however, also be noticeable by an error of fit at large times.

The finite length of the specimen may be used to advantage, if the heater strip extends to the edges of the specimen, the boundaries being perpendicular to the strips. In that case the heat current is forced to be perpendicular to the heater strip, thus eliminating the problem of finite length. In practice, however, the heat capacity of the solder points still contribute an error. The finite extension of the specimen perpendicular to the strips gives rise to a temperature perturbation, which may be estimated in terms of a reflected pulse from the boundaries. A simpler approach, often sufficient, is to consider the temperature increment at other boundaries than that carrying the strips, using Eq. (1) or the continuous line source. The error at the sensor is always smaller than the maximum of this quantity.

The distance, x, between the strips and their widths, w_h and w_s, are easily measured by a workshop microscope. The widths are obviously less critical, but a certain relative error in x gives rise to twice that error in thermal diffusivity. We measure the geometrical quantity x with an accuracy of ± 0.002 mm. In our experiments x is 1–2 mm, and hence the error in x contributes at most 0.4% error in the diffusivity. In addition to purely geometrical factors we must consider the possibility that the strips are nonuniform in thickness, especially across their widths. This can occur because of shadowing or solid angle effects on evaporation. These errors may be reduced to a tolerable level by mounting the mask symmetrically with respect to the evaporation source and sufficiently far from it.

Even if the heater strip is of uniform thickness, the power density may not be uniform. By plotting Eq. (1) we see that the temperature is uniform across the heater at small times and at large times. In an intermediate time range, however, the heater will be hotter at the center than at the edges. In view of the temperature coefficient of resistance this will lead to a power density slightly smaller at the center and larger at the edges, i.e., the temperature tends to be more uniform than indicated by Eq. (1). The

resulting error may be estimated by the following model. The perturbation caused by deviations from the average power density ($q/2w_h$) is represented by the quadrupole moment from a group of three line sources. Two of them are located at $0.75w_h$ from the center and dissipate $q_1(t)$. One is at the center and dissipates $-2q_1(t)$. The function $q_1(t)$ is obtained by simplest Simpson integration of Eq. (1) over the interval $0.5w_h < \xi < w_h$. The temperature perturbation at the sensor is then found by integrating over instantaneous line sources as in Eq. (8).

The power per unit length, q, is obtained from heater current, voltage drop, and distance between the voltage taps. The finite width of these taps, 0.15 mm in our case, introduces an uncertainty of about 0.8% in q and as much in λ. Photolithographic methods should make it possible to reduce this error by at least a factor of 10.

4.2. Error Related to Thermal Properties

The problem of the finite heat capacities of heater and sensor is treated in Sect. 2.3. Applied to our particular cases, with Ni and Cu strips 40–160 nm thick, these estimates give negligible contributions to the quantities measured. The theoretical expressions given in Sec. 2 are valid for a specimen in vacuum. The effect of a surrounding medium, such as air, may be roughly estimated by considering the heat diffusing into the specimen and into the medium, following a temperature step at the interface. A simple calculation shows the power transmitted in either direction to be proportional to $(\lambda\rho c_p)^{1/2}$. The error due to conduction in air would thus be about 0.02%, but convection could considerably increase this figure. The measurements were thus also performed in a vacuum, reducing the density by a factor of 1000. A comparison in the case of NaCl showed the change in λ caused by the air to be less than 0.03%, the value of ρc_p being unaffected.

The potential taps on the sensor connect the latter with a cooler region of the specimen. The measured temperatures could thus be expected to be too low. This error is difficult to estimate, but the following is a coarse attempt at a working model. The potential tap is considered as a thermal shunt over that part of the specimen on which it is deposited. The depth of the heated volume is of the order of the strip separation, x. If the thermal conductivity of the metal tap is denoted λ_m and its thickness d_m, the relative temperature error at the junction between tap and sensor may be written $\lambda_m d_m/\lambda x$, or 5×10^{-4} in our worst case. The error in the measured temperature, which is averaged over the sensor, is expected to be considerably smaller. Although our estimate is very uncertain, we are at least left with a satisfactory safety margin. The situation could be further improved by using potential taps of less conductive metal or alloy.

The temperature rise of the sensor in a typical experiment is about 1 K, and that of the heater is 2–5 K depending on the pulse duration chosen. Consequently the thermal properties are determined at a somewhat higher temperature than that measured before the onset of heating. Although we take this into account by calculating an average temperature over the active volume, there remains an uncertainty in temperature by a fraction of the heater temperature excursion. Bruce and Cannell [7] also discussed this problem and suggested a way of alleviating it.

Thermal transport by radiation may play a role at high temperature or, in rare cases, at room temperature and below. If the mean free path of infrared radiation is much smaller than the strip separation (x), the usual equation of heat conduction applies, and the effect of radiation is included in the measured conductivity. If the mean free path is of the order of x, the usual equation does not apply, and a poor fit may result. In such a case it is uncertain how measured conductivities should be interpreted. Finally, if the mean free path is much larger than x, power is lost directly from the heater to an extent that may be measured or estimated. In principle radiation from the heater may also proceed directly to the sensor, but fortunately the solid angle is vanishingly small in this geometry. It is thus sufficient to correct for radiative power loss from the heater to obtain the thermal conductivity.

4.3. Error Related to Electrical Properties

The main calibration problem is to relate accurately the sensor resistance, R, to the temperature, T. One problem is that the quartz thermometer used to measure T cannot, in practice, be clamped to the sensor strip. It actually measures the temperature of a copper box, in which the specimen is mounted. Our procedure is to keep the temperature constant for sufficiently long time to establish equilibrium. This is time-consuming but accurate, as judged from the resulting reproducibility. A more serious problem is the electrical stability of the evaporated sensor strip. It appears that R drifts noticeably over several days after evaporation, probably due to recrystallization. If the sensor is left to condition for a week at room temperature before calibration, however, we can determine the calibration factor, dR/dT, with a probable error of 0.2%. This factor then remains valid for many days, since dR/dT does not appear to drift.

A second calibration factor, dU/dR, is necessary to convert digitized lock-in amplifier voltages, U, to temperature. This calibration involves only electronic circuitry and is straightforward but must be repeated several times a day. An important point in certain situations is the time constant of the lock-in amplifier. In the measurements described in this paper we have set the voltmeter at the minimum time constant. Using a time constant of 1 ms, conductivitity values are observed to change by as much as 0.5%. The

total time constant of the instrument may be checked by suddenly changing ΔR to produce a step change of the lock-in amplifier output.

The quasistatic temperature calibration is strictly valid only under the original conditions, i.e., for constant temperature throughout the specimen. The calibration constant includes the effect of thermal expansion. Under pulse heating, however, the longitudinal thermal expansion of the sensor is reduced by the thermal stress field. In the worst case thermal expansion would be completely blocked during the pulse. The temperature coefficient, $R^{-1}dR/dT$, would then be smaller by an amount equal to the linear expansivity, α. The temperature coefficient for a metal at room temperature is typically $3 \times 10^{-3}\ K^{-1}$, and the expansivities of our specimens are in the range $(1 - 5) \times 10^{-5}\ K^{-1}$. The error in temperature, and hence in conductivity, should be less than 1% for quartz but may reach 2% for NaCl. In a real situation the thermal expansion is not completely blocked, which means that a smaller error generally can be expected.

Since the resistance, R, is measured at 1 kHz, skin effect must be considered. The skin depth [8] is given by $(\omega g \mu/2)^{-1/2}$, where ω = angular frequency, g = electrical conductivity, and μ = permeability. Using this formula we find that the skin depth is at least 1000 times the thickness of our sensor. The error due to skin effect should hence be vanishingly small.

4.4. Random Errors

The random errors of fit arise from the noise in the bridge circuits and from general interference. The propagation of the temperature scatter to the final results, λ and ρc, may depend on the choice of pulse time. The practical upper limit of the pulse time for a given geometry is set by end effects. We therefore investigated the effect of random errors by simulation, superimposing gaussian scatter on a theoretical temperature function (Eq. 2). The results show that precision is approximately independent of pulse time, at constant number of temperature points, as long as the pulse time exceeds $x^2 \rho c/\lambda$. Smaller times yield increased scatter of the measured data.

5. RESULTS AND DISCUSSION

5.1. Isotropic Case

We have already had occasion to study two isotropic materials using the two-strip method [2, 3], but since the objective then was to study possible changes caused by stress, we did not need to calibrate accurately. For the present tests we chose CaF_2, because it is easier to handle than NaCl. The specimen was a single crystal of pure CaF_2 from BDH Chemicals Ltd, Dorset, England. Its size was $50 \times 25 \times 25\ mm^3$, and strips were

Table I. Fitting Parameters for Single Crystal CaF_2[a]

	$A_1 = \lambda$ $(W \cdot m^{-1} \cdot K^{-1})$	$A_2 = \lambda/\rho c_p$ $(10^6\ m^2 \cdot s^{-1})$
Series 1	9.675 ± 0.004	3.491 ± 0.002
2	9.777 ± 0.002	3.516 ± 0.001
3	9.234 ± 0.004	3.578 ± 0.002
Mean	9.56 ± 0.17	3.53 ± 0.03

[a] Each series of measurements involves 10 heating events, fits being made to each temperature recording individually. The errors given are standard deviations of the mean. The mean temperature during pulses differed by a few K, but the results given here were reduced to 300 K assuming T^{-1} variation for λ and constancy for ρc_p.

deposited onto one of its larger faces according to Fig. 1. The strip separation was $x = 2.052$ mm, and the heating time per pulse 1.8 s.

Three series of measurements were made, each involving evaporation of strips and subsequent calibration of the temperature sensor. In each series we recorded 10 heating events and fitted the data. The standard deviation of the fits was 0.8 mK on the average, the temperature rise being 1.1 K. Table I lists the results of each series. The errors given after the parameter values are standard deviations of the mean, the standard deviations of the individual measurements being about three times larger. In the last row an average is taken of the three mean values above and a standard deviation calculated on the basis of these values.

We first note that the standard deviation of λ is 50 times larger for the total experiment than for a single series. This means that most of the uncertainty is associated with evaporation and thermometer calibration. As we see from the values of $\lambda/\rho c_p$, the standard deviation of the total result is about 15 times larger than for each series. As pointed out in Sec. 2.1, the parameter $\lambda/\rho c_p$ is independent of the thermometer calibration factor and depends only on the distance, x, and time.

Considering our known sources of error we thus expect to determine the thermal diffusivity, $\lambda/\rho C_p$, to an accuracy of better than 1%. The results from different series indicate, however, that systematic errors arise in connection with evaporation or calibration. Dividing the results for the two parameters, we obtain $\rho c_p = 2.710 \times 10^6\ J \cdot m^{-3} \cdot K^{-1}$ at 300 K, in good agreement with calorimetric measurements [9], which give $2.728\ J \cdot m^{-3} \cdot K^{-1}$. If we reverse the procedure and calculate λ from the diffusivity and the calorimetric value for ρc_p, we obtain $\lambda = 9.63\ W \cdot m^{-1} \cdot K^{-1}$, differing by 0.7% from the value determined virtually independently from the first fitting parameter. These facts strongly suggest that thermal conductivities

may be determined by this method with an accuracy of 2% or better in the isotropic case. A best fit to earlier results published by Slack [10] yields $\lambda = 9.4\ \mathrm{W \cdot m^{-1} \cdot K^{-1}}$ at 300 K with a probable error of several percent.

5.2. Anisotropic Case

A single crystal of α-quartz (SiO_2) was chosen for the anisotropic tests. The specimen was $34 \times 29 \times 17\ \mathrm{mm^3}$ and was cut perpendicular to the principal conductivity axes. Strip patterns were evaporated onto the two larger faces, the strips being parallel and perpendicular to the c axis, respectively. For symmetry reasons the thermal conductivity is the same in directions perpendicular to the c axis. Two different strip separations were used, $x = 1.349$ and 2.052 mm. For each separation we made three series of measurements involving evaporation and calibration. Each series consisted of 10 heating events. The standard deviation of the fits was 1.4 mK on the average for a temperature rise of 3 K. As with CaF_2 the individual measurements on SiO_2 exhibited very small standard deviation (about 0.1% in all cases). In Table II we list the average results, which have larger standard deviations, although they refer to the mean value. The reason for this increased scatter is the errors induced by evaporation and calibration.

For parallel orientation of the strips with respect to the c axis, λ_a is equal to λ_b by symmetry. We thus obtain these conductivity values directly from A_1, and ρc_p is equal to A_1/A_2. With λ_a, λ_b, and ρc_p known, we have, using the perpendicular orientation, $\lambda_c = A_2 \rho c_p$. We also obtain an additional value for one of the conductivities:

$$\lambda_b = A_1^2/\lambda_c\ .$$

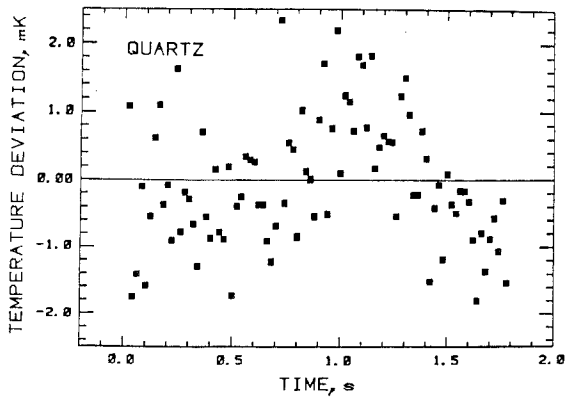

Fig. 5. Temperature deviation from the best-fitting theoretical function in the case of SiO_2. The standard deviation of the fit is 0.03% of the maximum temperature rise.

Table II. Fitting Parameters for Crystalline SiO_2 (α-Quartz)[a]

x	O	A_1 ($W \cdot m^{-1} \cdot K^{-1}$)	A_2 ($10^6\ m^2 \cdot s^{-1}$)
x_1	$\parallel$	$(\lambda_a\lambda_b)^{1/2} = 6.401 \pm 0.032$	$\lambda_a/\rho c_p = 3.277 \pm 0.008$
	$\perp$	$(\lambda_b\lambda_a)^{1/2} = 8.647 \pm 0.114$	$\lambda_c/\rho c_p = 5.871 \pm 0.013$
x_2	$\parallel$	$(\lambda_a\lambda_e)^{1/2} = 6.517 \pm 0.045$	$\lambda_a/\rho c_p = 3.310 \pm 0.009$
	$\perp$	$(\lambda_b\lambda_c)^{1/2} = 8.962 \pm 0.095$	$\lambda_c/\rho c_p = 5.946 \pm 0.041$

[a] Experiments were performed at two different strip separations (x). For each of these x values data were taken at two strip orientations (O), parallel ($\parallel$) and perpendicular ($\perp$) to the c axis. In each of these four cases an average of the fitting parameters is given. The average values are taken over three series of 10 measurements, each involving evaporation of strips and calibration of the resistance thermometer strip. The results are reduced to 300 K, and the errors are standard deviations of the mean. Strip separations were $x_1 = 1.349$ mm and $x_2 = 2.052$ mm.

In Table III we summarize the final results for SiO_2. We first notice that the mean specific heat capacity value agrees within 1% with results from adiabatic calorimetry [11]. The difference between our two mean values is also about as large as the combined random errors. For the conductivities, however, mean values generally differ by more than could be expected from the random errors given. This indicates that the strip separation (x) does influence the conductivity values, which theoretically should not occur. In particular the conductivity values obtained on the basis of adiabatically determined ρc_p differ more than expected, considering the estimated errors in x and in fitting. The results from the three series of

Table III. Final Values of Principal Thermal Conductivities and Heat Capacity per Unit Volume for Crystalline SiO_2 at 300 K[a]

x	$\lambda_a = \lambda_b$ ($W \cdot m^{-1} \cdot K^{-1}$)	λ_b ($W \cdot m^{-1} \cdot K^{-1}$)	λ_c ($W \cdot m^{-1} \cdot K^{-1}$)	ρc_p ($10^6 J \cdot m^{-3} \cdot K^{-1}$)
x_1	6.40 ± 0.03	6.52 ± 0.17	11.47 ± 0.03	1.95 ± 0.01
x_2	6.52 ± 0.05	6.86 ± 0.15	11.71 ± 0.08	1.97 ± 0.01
x_1	6.36 ± 0.02		11.39 ± 0.03	Known
x_2	6.42 ± 0.02		11.54 ± 0.08	Known

[a] Measurements were carried out at two strip separations, $x_1 = 1.349$ mm and $x_2 = 2.052$ mm. Two independent values of λ_b result from the analysis. The lower half of the table lists conductivity values obtained by combining the thermal diffusivity, A_2, with calorimetric results [11] for ρc_p.

measurements of A_2 which yield the mean values of Table III also scatter more than can be explained by errors in measuring x and in fitting. From the present experimental material, we must conclude that the quantities x, w_h, and w_s are not completely determined by measuring contour lines of the evaporated strips. It seems that uniformity across strips may not necessarily result from our evaporation procedure.

Our weighted mean value of ρc_p at 300 K is 1.958×10^6 J · m^{-3}K^{-1}, whereas adiabatic calorimetry [11] yields 1.94×10^6 J · m^{-3} · K^{-1}. Our weighted mean values of the principal thermal conductivities at 300 K are 6.40 and 11.44 W · m^{-1} · K^{-1}. Literature values of conductivities scatter considerably. The most recent publication on this subject [4] contains a review of earlier work. Concerning λ_a there is general agreement on a value of 6 . 5 W · m^{-1} · K^{-1}, but concerning λ_c there are essentially two groups of values. Birch and Clark [12] and Gustafsson et al. [4] agree about a value of $\lambda_c = 10.6$ W · m^{-1} · K^{-1}, although the latter group suggests the presence of an error in the case of the higher diffusivity. The results of Koenig [13], Colosky [14], and Kawada [15], on the other hand, extrapolate to an average of $\lambda_c = 11.4$ W · m^{-1} · K^{-1}. Comparison with earlier conductivity work thus does not give a definitive answer concerning the accuracy of our method. The agreement regarding ρc_p values as well as the internal consistency of the data presented in Table III lead us to believe, however, that our weighted thermal conductivity results are accurate to within 2% or better.

5.3. Conclusions

We have seen that a precision of 0.1% may be obtained in individual measurements and that considerable improvement over that figure is possible by taking mean values. The present method is thus a valuable tool in investigating small changes in thermal conductivity, such as that produced by uniaxial stress.

The most important systematic errors proved to be the following. End effects always arise at long pulse times but are revealed by inspection of the remainder after fitting. The time constant of the lock-in voltmeter did not contribute a significant error in the cases of CaF_2 and quartz. If higher thermal conductivities are to be measured, however, this error will probably become serious but may perhaps be taken into account by an inverse Laplace transform of the measured values. The quasistatic calibration of sensor resistance against temperature involved some difficulties. In order to achieve time stability of the sensor resistance, it became necessary to age the strips after evaporation. Bulk resistivity data from the literature cannot be used, since the temperature coefficients of evaporated metals are typi-

cally only half that of bulk metals. The problems caused by thermally produced stress (Sec. 4.3) were not investigated experimentally, but it seems probable that they could cause errors amounting to a large fraction of our estimated errors. An unexpected problem was the lack of uniformity across the strips, which effectively produced errors in measuring x, w_h, and w_s under the microscope. However, we have not explored the possibility that surface treatment can improve adherence, and improvements may also be possible by finding better strip materials.

The present accuracy of the two-strip method in specific heat capacity and thermal conductivity is 2% or better. The accuracy in cases of lower conductivities is expected to be as good, but with higher conductivities it depends on how well the time constant can be corrected for. Thermal diffusivity measurements by this method are particularly promising, since geometrical data and linear sensor characteristics are the only requirements. The accuracy in diffusivity would be brought to parts in 10^3, if the strips could be made narrower and their separation thus better defined. In order to reduce the associated large temperature excursions one could imagine using a semiconducting sensor material, having higher temperature sensitivity.

The advantage of the present method over the single-strip method (THS) [4] is two-fold. First, temperature data may be taken before switching on heat, which means that a superimposed, slow temperature variation need not produce errors. Secondly, the heat dissipation in the sensor is small and constant, which means that a possible thermal resistance at the interface would be of no consequence. This is of special importance in view of the possibility of extending the method to electrically conducting materials by interposing an insulation layer of, say, Ta_2O_5 [16] between the strips and the specimen.

ACKNOWLEDGMENTS

This work was financially supported by the Swedish Natural Science Research Council.

REFERENCES

1. G. Bäckström and J. Chaussy, *J. Phys. E: Sci. Instrum.* **10**:767 (1977).
2. U. Brydsten and G. Bäckström, *High Pressure Science and Technology*, B. Vodar and Ph. Marteau, eds. (Pergamon Press, Oxford, 1980), p. 217.
3. U. Brydsten, D. Gerlich, and G. Bäckström, *J. Phys. C: Solid State Phys.*, **16**:143 (1983).
4. S. E. Gustafsson, E. Karawacki, and M. N. Khan, *J. Appl. Phys.* **52**:2596 (1981).
5. P. R. Bevington, *Data Reduction and Error Analysis for the Physical Sciences* (McGraw-Hill, New York, 1969), p. 232.

6. H. S. Carslaw and J. C. Jaeger, *Conduction of Heat in Solids* (Oxford University Press, London, 1959), pp. 257, 59, 258.
7. H. Bruce and D. S. Cannell, *Rev. Sci. Instrum.* **47**:1320 (1976).
8. J. Reitz, F. Milford, and R. Christy, *Foundations of Electromagnetic Theory* (Addison-Wesley, Reading, Mass., 1979), p. 371.
9. S. S. Todd, *J. Am. Chem. Soc.* **71**:4115 (1949).
10. G. Slack, *Phys. Rev.* **122**:1451 (1961).
11. C. T. Anderson, *J. Am. Chem. Soc.* **58**:568 (1936)
12. F. Birch and H. Clark, *Am. J. Sci.* **238**:529 (1940).
13. J. H. Koenig, *Rutgers Univ. N. J. Ceram. Res. Sta. Progr. Rep.* **5**:1 (1954).
14. B. P. Colosky, *Am. Ceram. Soc. Bull.* **31**:465 (1952).
15. K. Kawada, *Bull. Earthq. Res. Inst.* **44**:1071 (1966).
16. A. Alloush, W. B. Gosney, and W. A. Wakeham, *Int. J. Thermophy.* **3**:225 (1982).